A NEW STACKING OPERATOR: i-CRS WITH 4 PARAMETERS

M. Bobsin, D. Gajewski, B. Schwarz and C. Vanelle

email: *martina.bobsin@zmaw.de*
keywords: *multiparameter stacking, i-CRS*

ABSTRACT

In applied seismics it is very important to get a first, reliable time image of the subsurface. So called multi-parameter stacking operators establish this image and in addition multiple important attribute sections. The quality of image and attributes strongly depends on the accuracy of the description of the traveltime moveout. The implicit common reflection surface (i-CRS) approach assumes a circular reflector beneath a heterogeneous medium. It leads to good results in terms of traveltime fit, coherence and attributes. By introducing a new degree of freedom to the i-CRS operator, we want to achieve a sensitivity improvement and a better fit, i.e. a larger coherence. The new free parameter is the overburden velocity. We investigate different four parameter approaches and compare the two most promising ones to the established three parameter methods CRS, planar MF and conventional i-CRS. The investigations include an accuracy study, a sensitivity study and the application as a stacking operator. All of them consider a simple synthetic model with different radii of curvature and different vertical velocity gradients. It turns out, that the new four parameter descriptions perform better in terms of traveltime fit and sensitivity than CRS, MF and i-CRS. The application as a stacking operator results in a slightly higher coherence and a worse attribute estimation compared with the three parameter i-CRS.

INTRODUCTION

Traveltime curves are derived for different seismic events like reflections, refractions and diffractions. These curves are approximated with different functions. The simplest one is a parabola. The stack sums up traces of the same regions in the subsurface (Mayne, 1962). Advantages of stacking are a reduction in the data volume and an improvement of the signal-to-noise ratio. New methods execute the stacking process in two directions. Subsurface information like the curvature of a reflector, are described by the kinematic wave field attributes α, R_{NIP} and R_N (Hubral, 1983). Different multiparameter stacking operators are applied. These are e.g. the shifted hyperbola (de Bazelaire, 1988), the common reflection surface (Müller, 1999), planar multifocusing (Gelchinsky et al., 1999) and the new approach of the implicit common reflection surface (Vanelle et al., 2010; Schwarz, 2011).

We investigate the extension of i-CRS up to four parameters. The fourth parameter is the overburden velocity. Simple synthetic models are considered to analyze the behavior of the four parameter i-CRS (i-CRS4) with respect to accuracy and sensitivity, and to compare the results with CRS, MF and i-CRS.

THEORY

Implicit common reflection surface

Vanelle et al. (2010) and Schwarz (2011) developed a new approach for multi-parameter stacking, i-CRS. The method is based on the assumption of a constant overburden velocity and can be expressed in terms of the CRS parameters. The problem of finding the reflection point on a circle is underlying. In Figure 1, the geometry of the problem is illustrated. The circle is described by the centre point (x_c, H) and the radius

R. The basic equations are the following ones:

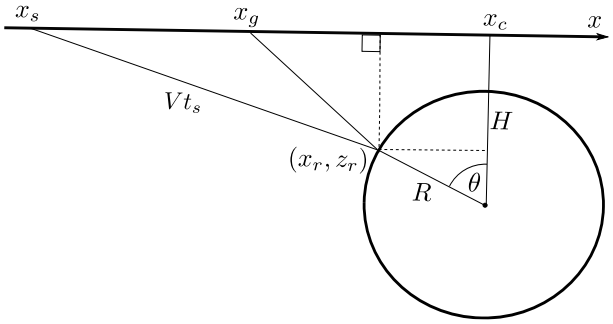

Figure 1: Based on the assumption of a homogeneous medium, the ray paths are straight. Due to symmetry, it only remains one unknown: the reflection angle θ.

$$t = t_s + t_g, \tag{1a}$$

$$t_s = \frac{1}{V}\sqrt{\left(x_m - h - x_c - R\sin(\theta)\right)^2 + \left(H - R\cos(\theta)\right)^2}, \tag{1b}$$

$$t_g = \frac{1}{V}\sqrt{\left(x_m + h - x_c - R\sin(\theta)\right)^2 + \left(H - R\cos(\theta)\right)^2}, \tag{1c}$$

$$\tan(\theta) = \frac{x_m - x_c}{H} + \frac{h}{H}\frac{t_s - t_g}{t_s + t_g}, \tag{1d}$$

$$\tan(\theta_0) = \frac{x_m - x_c}{H}. \tag{1e}$$

A strategy to calculate the reflection angle θ is suggested by Vanelle et al. (2010). We have to calculate θ_0 and insert it into the equations for t_s and t_g. Then calculate θ and repeat the procedure.

The connection to the CRS parameters is established by expanding the square of (1a) up to the second order and comparing the corresponding coefficients to their CRS counter parts (see Schwarz, 2011). For this task it is useful to make a transformation of coordinates. By introducing the following relations:

$$\sin(\tilde{\alpha}) = \frac{x_c}{\sqrt{{x_c}^2 + H^2}}, \tag{2a}$$

$$\tilde{R}_{NIP} = \sqrt{{x_c}^2 + H^2} - R, \tag{2b}$$

$$\tilde{R}_N = \sqrt{{x_c}^2 + H^2}. \tag{2c}$$

We end up with a system of four equations with four unknowns. The problem therefore is well-determined and its solution reads:

$$V = \frac{v_{NMO}}{\sqrt{1 + \frac{v_{NMO}^2}{v_0^2}\sin^2(\alpha)}}, \tag{3a}$$

$$x_c = -\tilde{R}_N \sin(\tilde{\alpha}) = \frac{-R_N \sin(\alpha)}{\cos^2(\alpha)\left(1 + \frac{v_{NMO}^2}{v_0^2}\sin^2(\alpha)\right)}, \tag{3b}$$

$$H = \tilde{R}_N \cos(\tilde{\alpha}) = \frac{v_0 R_N}{v_{NMO}\cos^2(\alpha)\left(1 + \frac{v_{NMO}^2}{v_0^2}\sin^2(\alpha)\right)}, \tag{3c}$$

$$R = \tilde{R}_N - \tilde{R}_{NIP} = \frac{\frac{v_0 R_N}{v_{NMO}\cos^2(\alpha)} - \frac{v_{NMO} t_0}{2}}{\sqrt{1 + \frac{v_{NMO}^2}{v_0^2}\sin^2(\alpha)}}, \tag{3d}$$

where $v_{NMO} = \sqrt{\frac{2 v_0 R_{NIP}}{t_0 \cos^2(\alpha)}}$ is the normal moveout velocity.

Four parameter extension

de Bazelaire (1988) and Thore et al. (1994) introduced the velocity as a free parameter.The multiparameter stacking operators (CRS, MF and i-CRS) do not include a free velocity. So we investigate the extension up to four parameter for i-CRS. We utilize some techniques from mathematics and physics, i.e. the expansion with zero (add and subtract), the multiplication with one (multiply and divide) and a simple substitution based on:

$$t_0 = \frac{2\tilde{R}_{NIP}}{V} = \frac{2\left(\sqrt{{x_c}^2 + H^2} - R\right)}{V}. \tag{4}$$

This relation results from the comparison of the zero-order coefficients of a Taylor series expansion. While introducing V and t_0 in equation(1a), we want to achieve, that small parameter deviations produce a maximum traveltime error. Finally we end up with different possible four parameter equations, which reads:

$$t = t_s + t_g + t_0 - \frac{2\tilde{R}_{NIP}}{V}, \tag{5a}$$

$$t = t_s + t_g + \exp(t_0) - \exp\left(\frac{2\tilde{R}_{NIP}}{V}\right). \tag{5b}$$

where the small letters a and b correspond to first and second traveltime equation, e.g. i-CRS4a.

ACCURACY STUDY

To investigate the accuracy, we consider a simple test model.

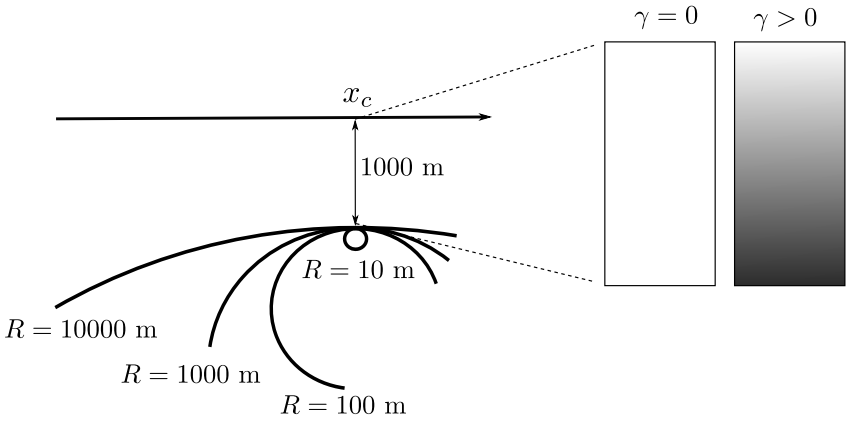

Figure 2: Evaluated are traveltimes for four different radii of curvature and four different vertical velocity gradients ($\gamma = 0, 0.5, 1, 1.5$ 1/s).

Beginning with $R = 10$ m representing the diffraction case, up to $R = 10000$ m, which marks a nearly planar reflector. The different vertical velocity gradients represent a homogeneous and inhomogeneous overburden.The midpoint displacement (Δx_m)and half-offset (h) range shall lie within realistic dimensions, i.e.

$$\Delta x_m = x_m - x_c \in [-2000, 2000]m, \quad h \in [0, 1000]m. \tag{6}$$

Each circle is located 1000 m below the surface, i.e. $H - R = 1000$ m. The errors as a function of midpoint displacement and half-offset are determined by the root-mean-square deviation:

$$\delta t_{RMS} = \sqrt{\frac{\sum_{i=1}^{n} \delta t_i^2}{n}}. \tag{7}$$

The variable n is the number of considered combinations of $(\Delta x_m, h)$, t_ref is the reference traveltime calculated with Seismic Unix (see Schwarz, 2011) and t_i denotes the respective operator traveltime. The

horizontal position of the center point x_c is placed in the centre of the aperture. Consequently, the angle of emergence vanishes, i.e. $\alpha = 0$, for all considered $(\Delta x_m, h)$ pairs, because of normal incidence. Thus, the operator traveltimes are estimated by minimizing (7). For the optimization of R_{NIP}, R_N and the fourth parameter V, we make use of the simplex search by Nelder and Mead (1965).

Figure 3 shows the results for the two four parameter extensions and conventional i-CRS3. The

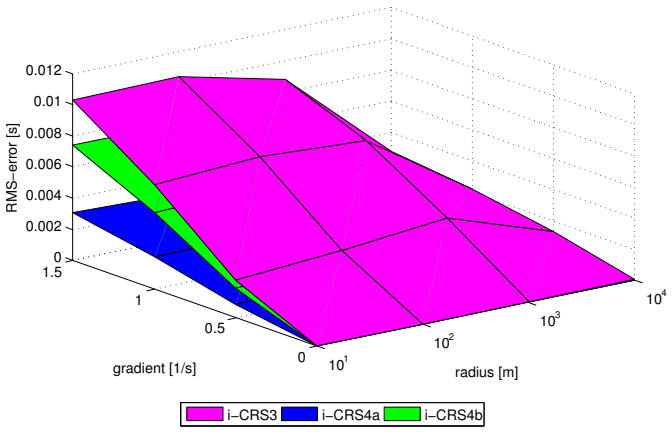

Figure 3: RMS-errors distribution for the three selected equations in dependency on radii of curvature and inhomogeneity. Please note the logarithmic radii scale.

blue surface (i-CRS4a) provides the smallest errors. Both four parameter equations offer a more precise traveltime fit for the case of an inhomogeneous overburden than i-CRS3. With increasing inhomogeneity the RMS-errors are increasing, too. For large radii the different i-CRS methods behave more similar.

Figure 4 shows the error distribution for a vertical velocity gradient of $\gamma = 0.5$ 1/s. For CRS we can see that the errors increase with higher half-offsets and midpoint displacements. The smallest errors for CRS are reached for $\Delta x_m = 0$, i.e. the CMP configuration. The shape and value of the error distribution of i-CRS3 and i-CRS4b is similar while i-CRS4a achieves the smallest errors. All i-CRS methods have in common, that the errors are biggest for a large midpoint displacement and offsets.

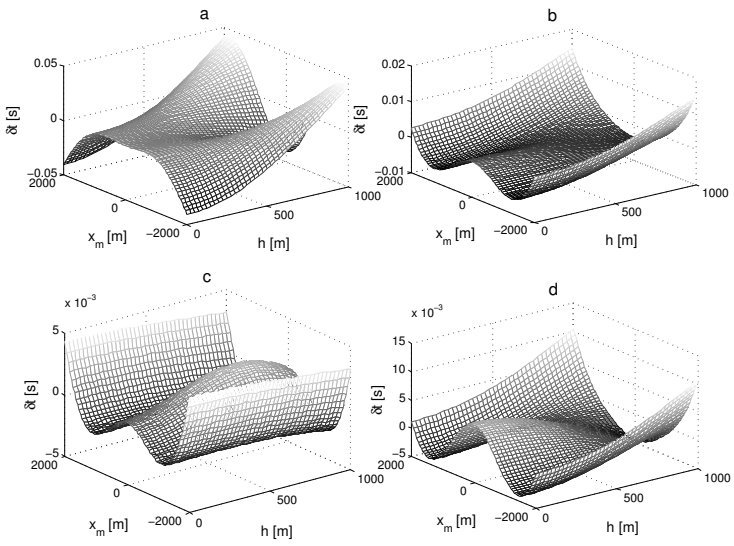

Figure 4: Traveltime error distribution of (a) CRS, (b) i-CRS3, (c) i-CRS4a, (d) i-CRS4b for an inhomogeneous overburden ($\gamma = 0.5$ 1/s) and $R = 1000$ m. Please note the different scales.

SENSITIVITY STUDY

In this part we take a closer look at the parameters and their behavior. The principle is very similar to Tygel et al. (2011). We choose a homogeneous model with the following model and acquisition parameters: $x_m \in [-1000, 1000]$ m, $h \in [0, 1000]$ m, $V = 2000$ m/s, $\alpha = 5°$, $R_{NIP} = 1000$ m and $R_N = 2000$ m. During the study we perturb the exact values of α, R_{NIP} and R_N, to simulate estimation errors. This is be done for two important configurations, the CMP gather ($\Delta x_m = 0$) and the zero-offset section ($h = 0$). One of the parameters is varied in steps of 2% from -10% to $+10\%$, while the remaining attributes are kept constant. This procedure reveals how the traveltime is affected by changing each of the parameters. We investigate the sensitivity for CRS, MF, i-CRS3, i-CRS4a and the i-CRS4b method. The aim of this study is that, if the traveltime varies much when a certain parameter is perturbed, we can infer that:

- this parameter can be accurately estimated, because we can distinguish between the correct and incorrect values,
- if this is not the case, the respective parameter for the invested equation is not sensitive and does not allow a good estimation.

Both Figures 5 and 6 show the traveltime deviation when the variation is applied to the exact values of α, R_{NIP} and R_N. Each curve represents the time deviation $\delta t = t - t_{ref}$, where t is the perturbed traveltime for the method and parameter under investigation and t_{ref} is the reference traveltime without variation. We start with the results of the perturbation for the common midpoint configuration ($x_m = 0$), as shown in Figure 5. For the perturbation of α, CRS shows the largest deviations, especially for large offsets. MF and i-CRS3 are worse than CRS. On the right side the values of the three i-CRS methods are the same and plotted on top of. In the case of R_{NIP}, the i-CRS4b has the largest time deviations across all offsets. In the CMP configuration i-CRS3 leads to better results than the i-CRS4a for R_{NIP}. For R_N, the largest deviations are achieved with MF followed by i-CRS3. Interesting is, that CRS shows no time deviation while varying R_N for $x_m = 0$. That is because the CRS equation (Müller, 1999) reduces to:

$$t^2(0, h) = t_0^2 + \frac{2t_0 \cos^2(\alpha)}{v_0} \frac{h^2}{R_{NIP}}. \tag{8}$$

This means that the determination of R_N can be done just imprecise. The i-CRS methods lead to the same results for α and R_N. For R_N, it is because the additional terms for the introducing of V in the four parameter equations (5) and the transformation equations (3) do not include R_N. In the case of α, we get the same results for a homogeneous medium ($V = v_0$ and $t_0 = \frac{2R_{NIP}}{v_0}$), because equation (4) contains only a R_{NIP} dependency (see Bobsin (2012)):

$$\frac{\sqrt{x_c^2 + H^2} - R}{V} = \frac{R_{NIP}}{v_0} \tag{9}$$

But if one consider an inhomogeneous medium the dependence on α does not vanish and one would see differences in the i-CRS methods, too.

The next Figure 6 shows the ZO configuration (h=0). The common intersection point of the curves is moved right because of $\alpha = 5°$. On the left side , we see that i-CRS3 is varying most. With larger values of x_m (positive and negative) the sensitivity increases, too. Interesting is that CRS and MF show no time deviation for R_{NIP}. That is because MF reduces for ZO to the parametric CRS (see Schwarz, 2011) and reads as follows:

$$t^2 = \frac{4}{v_0^2} \left(\Delta x_m^2 + 2\Delta x_m R_N \sin(\alpha) + R_N^2 \right). \tag{10}$$

The time deviation for the variation of α and R_N is again the same for all three i-CRS methods. The most important result is gained for R_{NIP}. Across all midpoints i-CRS4b has the largest time deviations, which means it is very sensitive towards the estimation of R_{NIP}. But also i-CRS4a shows larger deviations than i-CRS3 and therefore for CRS and MF for a certain parameter perturbation.

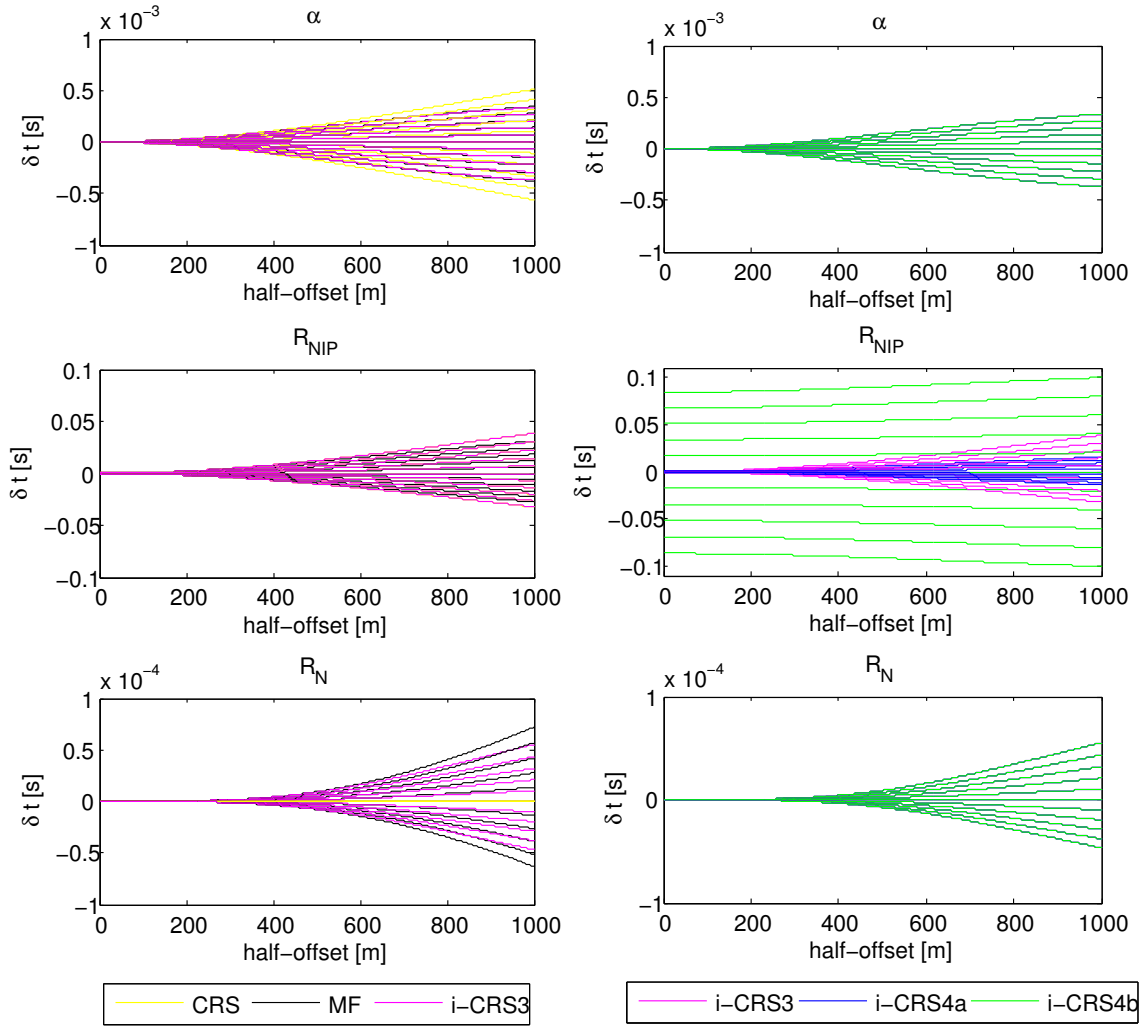

Figure 5: Sensitivity for three parameter methods (left) and i-CRS methods (right) for a CMP configuration.

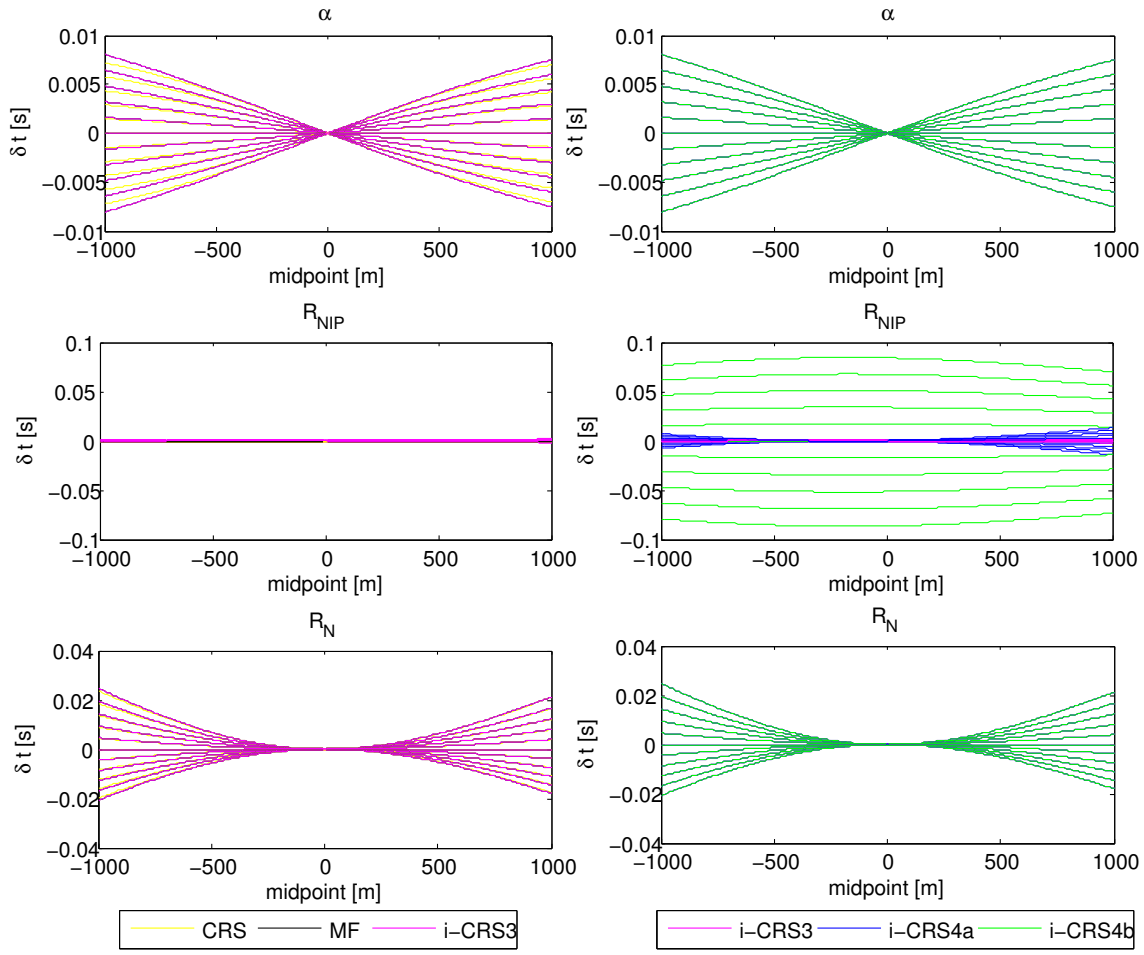

Figure 6: Sensitivity for three parameter methods (left) and i-CRS methods (right) for a ZO configuration

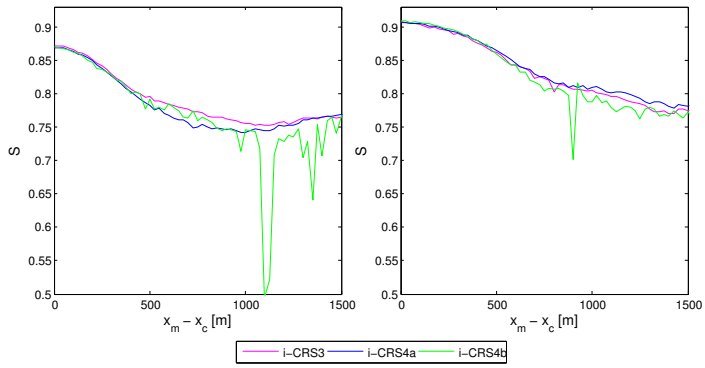

Figure 7: Semblance for $R = 100$ m and the i-CRS methods. On the left side is a homogeneous medium considered and on the right side an inhomogeneous with $\gamma = 0.5$ 1/s.

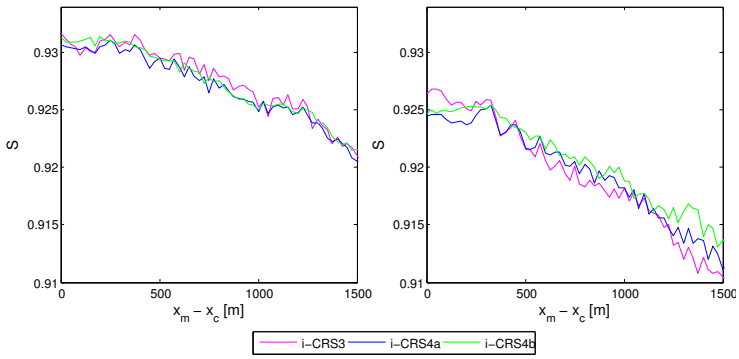

Figure 8: Semblance for $R = 10000$ m and the i-CRS methods. On the left side, a homogeneous medium is considered and on the right side an inhomogeneous medium with $\gamma = 0.5$ 1/s.

SYNTHETIC DATA EXAMPLE

Here we want to verify, whether the good results from the accuracy and sensitivity study can also be confirmed for the stacking. We apply i-CRS4a and i-CRS4b as stacking operators on the extended CRS implementation by Mann (2002). The underlying model is shown in Figure 2. In contrast to the accuracy study, where the RMS-error of the operator traveltime is minimized, the key task of the stacking routine is to maximize coherence. To measure the coherence one can make use of the semblance coefficient (Taner and Koehler, 1969).Schwarz (2011) showed the comparison of the semblance for CRS, MF and i-CRS3. There i-CRS leads to the largest values for all different considered radii of curvature and vertical velocity gradients. So we investigate the behavior of the different i-CRS methods.

Figure 7 shows the semblance for a strongly curved reflector. The i-CRS3 has the largest values, while i-CRS4b fluctuates for larger midpoint displacements ($x_m - x_c$) from the circle's center. In the case of inhomogeneity, i-CRS4a has the largest values. For small midpoint displacements all methods show a similar behavior. In general, the semblance values are larger for all methods in this region and the fluctuations of i-CRS4b are suppressed. Figure 8 shows the semblance for the nearly planar reflector case. Only small deviations between the i-CRS methods can be seen. The values are larger than for $R = 100$ m and no fluctuations for i-CRS4b can be found.

Figures 9 to 11 show the estimated kinematic wave field attributes. The semblance shows nearly no influence of vertical velocity gradients. Therefore we only present the results for a homogeneous medium. Figure 9 shows that α is better estimated for larger radii of curvature. The different i-CRS methods are similar for $R = 10000$ m and differ for $R = 100$ m. Figure 10 shows the calculated values for R_{NIP}.

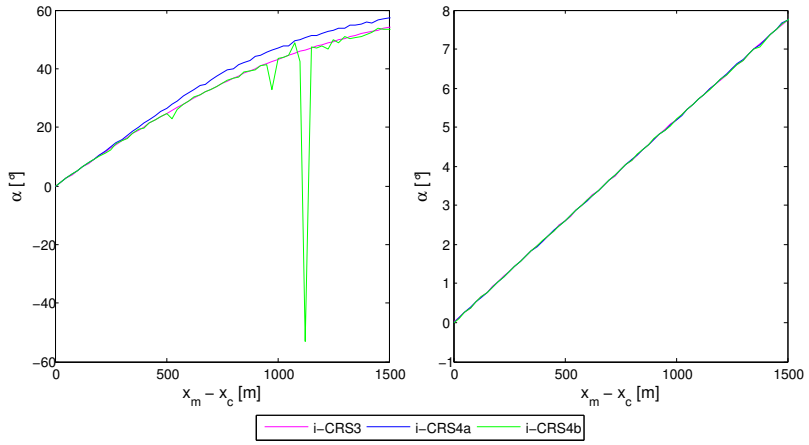

Figure 9: Values for the parameter α are shown for $R = 100$ m (left) and $R = 10000$ m (right). Please note the different scales.

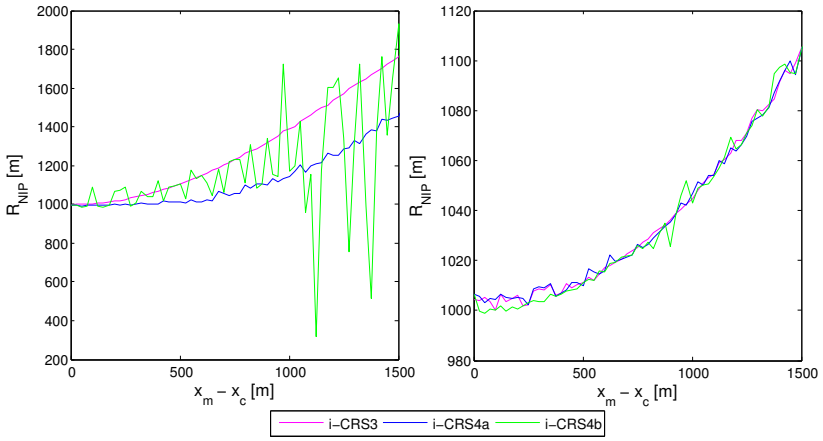

Figure 10: Values for the parameter R_{NIP} are shown for $R = 100$ m (left) and $R = 10000$ m (right). Please note the different scales.

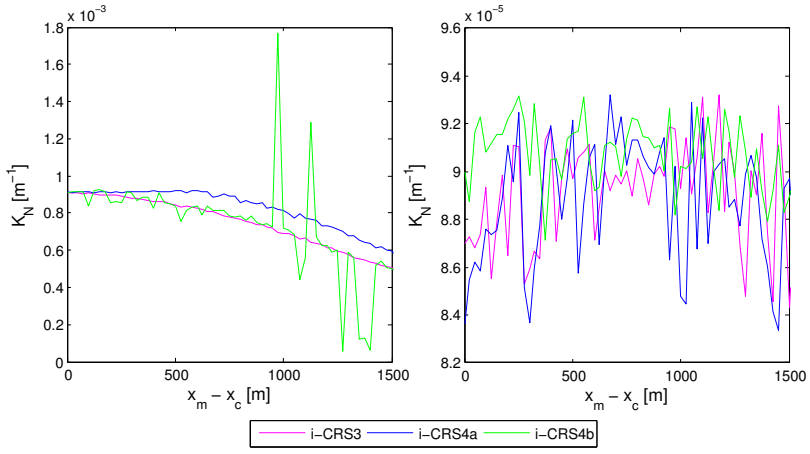

Figure 11: Values for the parameter R_N are shown for $R = 100$ m (left) and $R = 10000$ m (right). Please note the different scales.

For the strong curvature case i-CRS4b fluctuates between i-CRS3 (top) and i-CRS4a (bottom). Again the values for the nearly planar reflector are very similar. Instead of R_N we show its inverse K_N, because infinite values cannot be illustrated in a moderate way. For $R = 100$ m the curve of i-CRS4b is close to the corresponding counterparts of i-CRS3, whose values are smaller than for i-CRS4a.

CONCLUSIONS AND OUTLOOK

We investigated a four parameter i-CRS equation and their behavior in comparison with existing three parameter approaches (CRS, MF and i-CRS). The accuracy study shows a smaller errors for all considered four parameter approaches with respect to reference traveltimes. Overall i-CRS4a shows the smallest deviations for all considered scenarios. The main result of the sensitivity study is that all i-CRS formulae are more sensitive than CRS and MF in the CMP configuration and ZO section. Highest sensitivities for R_{NIP} are reached for i-CRS4b. The synthetic data example shows small deviations between the i-CRS methods. Semblance and attribute estimates are very smooth for i-CRS4a, while for i-CRS4b they considerably fluctuate, especially for small radii of curvature. Surprisingly, the i-CRS4a search turned out to be more economical in terms of computational time than i-CRS3 about 5% for the simple models under investigation.

In future more complex and realistic subsurface models have to be investigated. It might be also conceivable to look for further four parameter extensions, which allow to systematically steer the sensitivity of the operator.

ACKNOWLEDGMENTS

We want to thank all persons who directly or indirectly contributed to this work. This work was kindly supported by the sponsors of the *Wave Inversion Technology (WIT) Consortium*.

REFERENCES

Bobsin, M. (2012). A new stacking operator: i-CRS with 4 parameters. Bachelor's thesis, University of Hamburg.

de Bazelaire, E. (1988). Normal moveout revisited: Inhomogeneous media and curved interfaces. *Geophysics*, 53:143–157.

Gelchinsky, B., Berkovitch, A., and Keydar, S. (1999). Multifocusing homeomorphic imaging - part 1. basic concepts and formulae. *Journal of Applied Geophysics*, 42:229–242.

Hubral, P. (1983). Computing true amplitude reflections in a laterally inhomogeneous earth. *Geophysics*, 48:1051–1062.

Mann, J. (2002). *Extensions and Applications of the Common-Reflection-Surface Stack Method*. PhD thesis, University of Karlsruhe.

Mayne, W. (1962). Common reflection point horizontal data stacking techniques. *Geophysics*, 27:927–938.

Müller, T. (1999). *The Common Reflection Surface stack method - Seismic imaging without explicit knowledge of the velocity model*. PhD thesis, University of Karlsruhe.

Nelder, J. and Mead, R. (1965). A simplex method for function minimization. *Computer Journal*, 7:308–313.

Schwarz, B. (2011). A new nonhyperbolic multi-parameter operator. Master's thesis, University of Hamburg.

Taner, M. T. and Koehler, F. (1969). Velocity spectra - digital computer derivation and applications of velocity functions. *Geophysics*, 34:859–88.

Thore, P., de Bazelaire, E., and Ray, M. (1994). The three-parameter equation: An efficient tool to enhance the stack. *Geophysics*, 59:297–308.

Tygel, M., Perroud, H., Lopes, R., and Krummenauer, R. (2011). Sensitivity of the non-hyperbolic common reflection surface. *15th WIT Report*, pages 333–342.

Vanelle, C., Kashtan, B., Dell, S., and Gajewski, D. (2010). A new stacking operator for curved subsurface structures. *80th Ann. Int. Mtg. Soc. Expl. Geoph.*